JGR Earth Surface

RESEARCH ARTICLE
10.1029/2026JF009129

Predicting Riparian Seedling Removal: A Mechanistic Scour Model Supported by Lab and Field Evidence

Elowyn M. Yager[1], Walter Bertoldi[2], Annunziato Siviglia[2], Elena Chenet[2], and Andrew W. Tranmer[1]

[1]Department of Civil and Environmental Engineering, Center for Ecohydraulics Research, University of Idaho, Boise, ID, USA, [2]Department of Civil, Environmental and Mechanical Engineering, University of Trento, Trento, Italy

Key Points:

- Root-sediment friction varies with grain size distribution, root irregularities, and lateral root area
- Accurate root resisting forces require root-sediment friction estimates, vertical changes in taproot diameter, and root hair effects
- Critical scour depths for seedling pullout vary with bed grain size, flow magnitude, and seedling biomass properties

Supporting Information:

Supporting Information may be found in the online version of this article.

Correspondence to:

W. Bertoldi,
walter.bertoldi@unitn.it

Citation:

Yager, E. M., Bertoldi, W., Siviglia, A., Chenet, E., & Tranmer, A. W. (2026). Predicting riparian seedling removal: A mechanistic scour model supported by lab and field evidence. *Journal of Geophysical Research: Earth Surface*, *131*, e2026JF009129. https://doi.org/10.1029/2026JF009129

Received 23 JAN 2026
Accepted 7 JUL 2026

Author Contributions:

Conceptualization: Elowyn M. Yager, Walter Bertoldi, Annunziato Siviglia, Andrew W. Tranmer
Funding acquisition: Elowyn M. Yager, Walter Bertoldi
Investigation: Elowyn M. Yager, Walter Bertoldi, Annunziato Siviglia, Elena Chenet, Andrew W. Tranmer
Methodology: Elowyn M. Yager, Walter Bertoldi, Annunziato Siviglia, Elena Chenet, Andrew W. Tranmer
Project administration: Elowyn M. Yager, Walter Bertoldi
Software: Elowyn M. Yager

Abstract Riparian seedlings growing on river bars, islands, and floodplains create feedback processes with hydraulics, sediment transport, and channel morphodynamics. For example, intact seedling uprooting by the flow typically requires some degree of sediment scour before seedling removal. Estimates of the critical scour depth (L_c) that allows for individual seedling uprooting are often based on the resisting root force (F_P). We develop a new mechanistic F_P equation that includes root-sediment friction from different grain size distributions, root irregularities, and lateral root areas. Simple laboratory experiments demonstrate that root-sediment friction coefficients from previous studies may be orders of magnitude lower than those that occur in riparian areas with coarse grain size distributions. We test different forms of our equation using field measured F_P to find that accurate F_P predictions require: (a) a range of root-sediment frictional effects, (b) declining taproot diameter with below ground distance, and (c) root hair effects. Combining our F_P equation with simple flow calculations, we calculate that L_c for an individual seedling is not constant as often assumed but depends on the bed grain size distribution, flow conditions, aboveground seedling patch density, and belowground and aboveground individual seedling biomass properties. We calculate similar L_c for invasive and native seedling species, suggesting that invasive seedling removal through targeted high-flow dam releases requires careful consideration of potential effects on native seedlings.

Plain Language Summary Vegetation growing in and along rivers affects river stability, river shape, flooding, and habitat for other organisms. Newly established vegetation can be pulled out by the river flow only if sediment erosion first occurs around the vegetation, which reduces the root-related forces holding vegetation in place. We develop a new equation to predict these root related forces and the amount of erosion that is needed for vegetation removal by the flow. We find that the friction between roots and surrounding sediment can vary with the sediment size, irregularities in the root shape, and root areas. Accurate root force predictions are required including these root-sediment friction effects as well as root diameter changes belowground and root hair impacts. The erosion depths needed for vegetation removal were not constant as often assumed and could vary with characteristics of the sediment, flow, and vegetation itself. We calculated that invasive and native vegetation species can have similar scour depths for removal, which has implications for invasive species removal strategies in rivers.

1. Introduction

Within fluvial systems, riparian vegetation can significantly impact flow hydraulics (Boothroyd et al., 2016; Curran & Hession, 2013; Chen et al., 2012; Nepf, 1999), sediment transport (Bouma et al., 2007; Yager & Schmeeckle, 2013; Yang et al., 2016; Zong & Nepf, 2011), and resulting channel morphodynamics (Bertoldi et al., 2014; Bywater-Reyes et al., 2017; Gurnell et al., 2019; Li et al., 2022; Tranmer et al., 2024). These physical processes, in turn, affect the initial recruitment, stability, and fitness of individual plants as well as the diversity of riparian ecosystems (Braatne et al., 1996; Caponi et al., 2019; Cooper et al., 1999; Corenblit et al., 2016; Shafroth et al., 1995; Tranmer et al., 2020). Some of the complex feedback mechanisms between riparian vegetation and physical processes are included in 1D and 2D morphodynamic models (Bertoldi et al., 2014; Caponi & Siviglia, 2018; Li et al., 2022; Solari et al., 2016; Yamasaki et al., 2019). However, uncertainties remain on how to best capture these feedback mechanisms, particularly for flow induced removal of seedlings. This can be critical in river restoration projects, where planted seedlings are often used to increase bank strength, augment future channel shading, and restore native vegetation populations. Whether such planted seedlings will be stable during floods is largely neglected. Other restoration projects target manual or flow-induced removal of non-native

Supervision: Walter Bertoldi
Validation: Elowyn M. Yager, Walter Bertoldi, Elena Chenet, Andrew W. Tranmer
Visualization: Elowyn M. Yager
Writing – original draft: Elowyn M. Yager
Writing – review & editing: Elowyn M. Yager, Walter Bertoldi, Annunziato Siviglia, Andrew W. Tranmer

seedlings owing to their potential negative effects on ecological function, channel morphology, and native vegetation (Belote et al., 2010; Elliott et al., 2019; Johnson, 1997; Shafroth et al., 2010). Therefore, predictions of flow-induced seedling removal are important for fundamental channel morphodynamics and applied river management.

During high-flow events, individual seedling root resistance typically exceeds the fluid forces on a plant's aboveground biomass and therefore, some degree of sediment scour is usually required for flow induced removal (Bau' et al., 2019; Bywater-Reyes et al., 2015; Calvani et al., 2019; Edmaier et al., 2015; Taye et al., 2026). Sediment scour can be locally caused by individual stems (Wu et al., 2021; Yager & Schmeeckle, 2013) or can occur at larger spatial scales (e.g., patch, bar, reach) (Rominger et al., 2010; Taye et al., 2026; Tranmer et al., 2024; Vargas-Luna et al., 2019), the latter of which is our focus. Individual seedling removal with sediment scour occurs when fluid forces exceed either the: (a) root-sediment frictional forces (F_P), which results in plant uprooting and pullout of an intact root system, or (b) root tensile strength, which causes taproot breakage and root pullout above the breakage point. The critical scour depth required for individual seedling removal (L_c) is calculated by balancing fluid forces with root resisting forces (Bau' et al., 2019; Bywater-Reyes et al., 2015; Calvani et al., 2019). To predict vegetation effects on channel migration and stability, morphodynamic models often require some estimate of L_c for individual seedlings or patches of seedlings (Bertoldi et al., 2014; Caponi & Siviglia, 2018).

Significant uncertainties remain in estimating L_c for individual seedling uprooting partly because predicting F_P can be challenging. Relatively simple mechanistic equations for single seedlings (Calvani et al., 2019), more complex mechanistic root bundle models (Pollen & Simon, 2005; Pollen-Bankhead & Simon, 2009; Schwarz et al., 2010), or empirical fits between measured pullout forces and seedling characteristics (Bau' et al., 2019; Bywater-Reyes et al., 2015) have all been used to determine F_P. In particular, uncertainties remain in how to represent the effects of: (a) variable taproot diameters, (b) root-sediment friction, (c) lateral roots, and (d) root hairs.

Equations using vertically constant (Calvani et al., 2019; Zhu et al., 2022) or vertically decreasing (Schwarz et al., 2010) taproot diameters both provide reasonable F_P predictions, making it unclear if taproot diameter changes with depth are important. Root-sediment friction effects are also not systematically parameterized; they have been estimated from ropes/wood/steel/rubber pulled out of soil/sand mixtures (Calvani et al., 2019; Schwarz et al., 2011; Zhu et al., 2022) or from simple sediment friction angles (Schwarz et al., 2010). Measured F_P can vary with the bed grain size distribution (GSD) (Bywater-Reyes et al., 2015) likely because of GSD dependent sediment friction angles (Yager et al., 2018) and root-sediment friction coefficients (Schwarz et al., 2010). However, root-sediment friction has only been estimated for relatively fine grain sizes (sand or smaller) that is not representative of the wider range of potential alluvial GSDs (e.g., sand vs. cobble-gravel) in which riparian vegetation (e.g., *Populus, Salix, Tamarix*) grows. Although some equations account for frictional resistance at root junctions (Schwarz et al., 2010), most use smooth cylindrical roots. Such simplified root models do not include root irregularities such as changes in root diameter, path, or shape caused by impenetrable obstacles such as large rocks (thigmotropism) (Kolb et al., 2017; Martins et al., 2020; Silverberg et al., 2012).

The area and configuration of lateral roots can also affect F_P (Mickovski et al., 2007; Schwarz et al., 2011), which are included directly in root bundle models (Schwarz et al., 2010; Zhu et al., 2022). Despite the advantages of such models, they typically contain many difficult to measure variables and do not include scour effects on F_P, thereby rendering them impractical for L_c estimates in morphodynamic models. Conversely, simple mechanistic F_P equations incorporate lateral roots as a greater number of total roots without accounting for potentially important variables such as lateral root areas, lateral root diameters, or lateral root burial depths (Calvani et al., 2019). Finally, although root hairs are important for water and nutrient uptake (Cai & Ahmed, 2022), their effects on seedling stability and F_P are uncertain; root hairs have been shown to significantly increase F_P (De Baets et al., 2020) or have no measurable effect (Bailey et al., 2002).

To address these uncertainties, we develop a simple mechanistic F_P equation for individual seedlings that includes: (a) vertical taproot diameter changes, (b) effects of grain size distribution, root shape irregularities, and lateral roots on root-sediment friction coefficients, (c) root hair effects, and (d) sediment scour induced reductions in buried root areas. We quantify root-sediment friction coefficients using laboratory experiments in which we measure F_P for simulated roots with different shapes, bed GSD, and lateral root areas. We test our equation using field measurements of F_P and previously published data that include manual scouring around seedlings. We

finally couple our F_P equation with equations for fluid forces on individual plants to predict differences in scour susceptibility between native and non-native riparian species in the USA.

2. Methods

2.1. Pullout Forces, Drag Forces, and Critical Scour Depths

We developed a system of equations to predict L_c for individual seedlings that may be growing within patches of vegetation or could be isolated on the riverbed. We assumed that within a patch of vegetation, root-sediment friction and F_P for an individual seedling were not influenced by roots of other seedlings within the patch and that pullout occurred rather than breakage because the root tensile strength exceeded F_P. Although soil strength can be influenced by roots from multiple plants (Pollen & Simon, 2005; Schwarz et al., 2010), the interacting effects of multiple seedlings on root-sediment friction within coarse alluvial sediment (e.g.., sand and gravel) are unknown and require further investigation. Conversely, our calculations included the effects of vegetation patch density on the fluid forces experienced by an individual seedling within a patch. Such effects have been well studied and can be predicted using equations for flow through vegetation patches.

2.1.1. Pullout Force Equations

To predict F_P, we started with the Mohr-Coulomb law for saturated sediment

$$\tau_s = c + [\sigma - u_w] \tan \phi \tag{1}$$

where τ_s is the sediment shear strength, c is the sediment cohesion, σ is normal stress, u_w is the pore water pressure, $\sigma - u_w$ is the effective stress, ϕ is the sediment friction angle (Table 1). We generally ignored cohesion ($c = 0$) given that we are focused on gravel-bedded rivers dominated by coarse sediment. Following Calvani et al. (2019), we determined F_P as the product of the sediment shear strength, root-sediment friction coefficient (f), and the taproot area that remains for a given assumed erosion depth (L_e) (Figure 1). Our F_P equation accounts for root hair resistance and a declining taproot diameter (D_T) with vertical distance below the bed surface (z). Assuming a constant D_T overpredicted F_P (see results section) because the largest overlying sediment weight occurred at high z where D_T was actually very small. We defined F_P as

$$F_P = \pi[\rho_s - \rho_w][1 - \lambda]\, g \tan \phi [1 + C_{\mathrm{RH}}] \int_{L_e}^{L_T} [z - L_e]\, D_T(z) f(L_e)\, \mathrm{d}z \tag{2}$$

where L_T is total vertical taproot length, ρs is sediment density, ρw is water density, g is gravitational acceleration, and λ is sediment porosity (Table 1). We included a root hair resistance term ($C_{\mathrm{RH}} = 1.18$), which is the ratio of the force due to root hairs alone to the force from roots without hairs using data from Da Baets et al. (2020) (see Figure S1 in Supporting Information S1). We integrated Equation 2 between L_e and L_T to obtain the pullout force that results from a given scour depth; when $L_e = 0$, this is equivalent to integrating between the bed surface ($z = 0$) and the bottom of the taproot.

We estimated $D_T(z)$ using a dimensionless linear function

$$\frac{D_T(z)}{D_T(0)} = \frac{D_T(z)}{D_S} = -0.99 \frac{z}{L_T} + 1 \tag{3}$$

in which we assumed that: (a) D_T at $z = 0$ is equal to the seedling stem diameter (D_S) at the bed surface, and (b) D_T linearly decreases with z and reaches $0.01 D_S$ at the taproot end ($z = L_T$).

We did not include lateral roots directly in Equation 2 because of the large amount of information required to properly do so. For example, we would need to know the exact number of lateral roots, the vertical position at which the lateral root begins, the angle of the lateral root from horizontal, the starting diameter of the lateral root, the length of the lateral root, and the change in the lateral root diameter along its length. We instead indirectly included the effects of lateral root area (A_{LR}) through f (see Sections 2.2 and 3.1) and incorporated the effects of lateral root scour by making f a function of the scour depth ($f(L_e)$).

Table 1
Symbol Legend

a	Projected vegetation patch area per volume
A_c	Frontal canopy area exposed to the flow
A_{LR}	Lateral root area before any scour
$A_{\mathrm{LR}}(L_e)$	Lateral root area for a given scour depth
c	Cohesion
C_D	Seedling drag coefficient
C_P	Seedling pronation correction to reduce F_D
C_{RH}	Root hair resistance term
D_S	Stem diameter at bed surface
D_{SEQ}	Stem equivalent diameter
$D_T(z)$	Taproot diameter at a given z
g	Gravitational acceleration
GSD	Grain size distribution of bed
H_C	Canopy height
h	Flow depth
f	Root-sediment friction coefficient
F_D	Drag force on seedling
F_P	Root force resisting seedling pullout
L_c	Critical scour depth; $L_c = L_e$ in Equation 2 when $F_P = F_D$
L_e	Assumed/measured scour depth for F_P calculations
L_T	Taproot length
m	Number of seedlings per unit bed surface area
S	Energy slope
$\overline{u}$	Vertically averaged velocity over canopy height
$u(Z)$	Velocity at Z distance above the bed
u_w	Pore water pressure
w_c	Volumetric water content of sediment
z	Vertical distance below the ground surface
Z	Vertical distance above the ground surface
ϕ	Sediment friction angle
λ	Sediment porosity
ρ_w	Water density
ρ_s	Sediment density
σ	Normal stress
τ	Reach-averaged shear stress
τ_{cg}	Critical shear stress for gravel
τ_{cs}	Critical shear stress for sand
τ_{s}	Sediment shear strength

2.1.2. Drag Force Equations

The critical scour depth needed for seedling removal (L_c) is equal to L_e in Equation 2 when the drag force on the seedling (F_D) equals F_P (Bau' et al., 2019; Bywater-Reyes et al., 2015; Calvani et al., 2019). We ignored seedling buoyancy and the drag force on any exposed roots after scour, which we assumed to be small or removed by the flow. Buoyancy calculations required volumes of leaves and stems, which were not readily available but could be

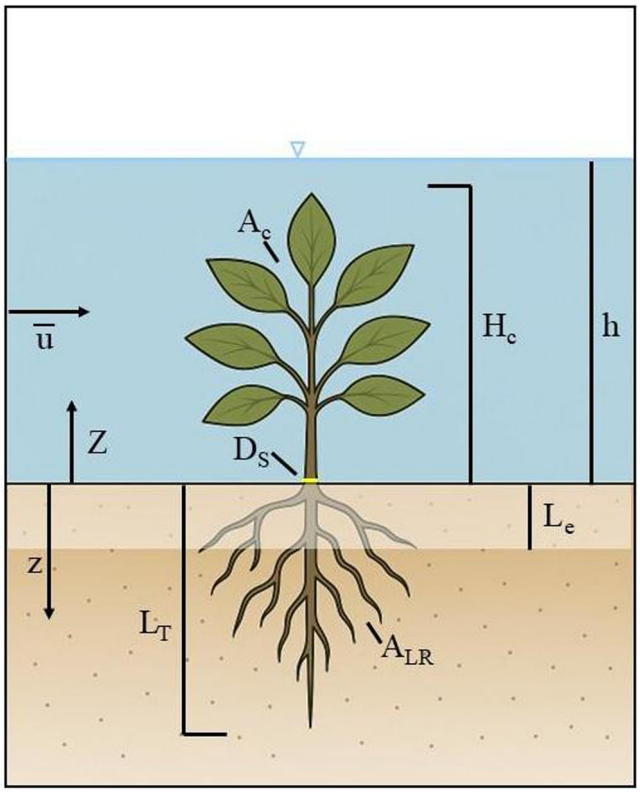

Figure 1. Conceptual diagram of seedling including the stem diameter (D_s), taproot length (L_T), lateral root area (A_{LR}), canopy area (A_c), canopy height (H_c), flow depth (h), flow velocity averaged over the plant height ($\overline{u}$), vertical distance belowground (z), vertical distance aboveground (Z), and assumed erosion depth (L_e). Figure background image generated with Microsoft Copilot.

estimated in the future using allometric equations. The drag force on an individual seedling's aboveground canopy is

$$F_D = \frac{1}{2}\rho C_D A_C \overline{u}^2 C_P \tag{4}$$

where C_D is the individual seedling drag coefficient, A_c is the individual seedling frontal canopy area (Figure 1), $\overline{u}$ is the vertically averaged flow velocity within a vegetation patch, and C_P is a correction factor to account for potential seedling pronation following Bywater-Reyes et al. (2015) (Table 1). Downstream oriented/pronating seedlings may require higher scour depths than those oriented upstream or vertically (Taye et al., 2026) because pronation likely reduces F_D. We used a velocity profile equation for flow through a submerged vegetation patch (Defina & Bixio, 2005), neglecting the portion of the profile above the vegetation

$$u(Z) = \sqrt{\frac{2gS}{\beta\left(G/H_C^2\right)}\left[\left(\frac{h}{H_C}-1\right)\frac{\sinh\left(\frac{\beta Z}{H_C}\right)}{\cosh(\beta)}+\frac{1}{\beta}\right]} \text{ for } 0 < Z \le H_C \tag{5}$$

where u is the flow velocity at Z vertical distance above the bed surface and

$$G = 0.0144\sqrt{hH_C} \tag{6}$$

$$\beta = \sqrt{\frac{aC_D H_C}{G/H_C}} \tag{7}$$

and S is energy slope, h is flow depth, and H_C is canopy height (Figure 1). The projected vegetation patch area per volume (a) is provided by

$$a = mD_{\mathrm{SEQ}} \tag{8}$$

where m is the number of plants in the patch per unit bed surface area and D_{SEQ} is the stem equivalent diameter of the plants. For simplicity, we assumed that all seedlings within the vegetation patch are the same size as the individual seedling of interest for which we are calculating pullout removal. Normally Equation 8 uses D_S instead of D_{SEQ} by assuming plants lack foliage but to implicitly account for canopy foliage we determined D_{SEQ} as

$$D_{\mathrm{SEQ}} = A_C/H_C \tag{9}$$

Finally, $\overline{u}$ is given by the integral of Equations 5 over the canopy height

$$\overline{u} = \frac{1}{H_C}\int_0^{H_C} u(Z)\,\mathrm{d}Z \tag{10}$$

Grain roughness effects on the velocity profile are often neglected in flow through vegetation (Nikora et al., 2013; Yang et al., 2015) and we assumed that differences in bed GSD will not significantly alter $\overline{u}$.

2.1.3. Predictions of F_P or L_c

To predict F_P using Equations 2 and 3, we required estimated values of f, which we obtained in Sections 2.2 and 3.1, and measured values of ϕ, L_e, D_S, L_T, and A_{LR}. To instead predict L_c for a given flow condition, we iterated Equations 2–10 to solve for L_c ($L_c = L_e$) using estimated values of ϕ, D_S, L_T, A_{LR}, S, h, m, H_C and A_C, and assumed values of C_p (see SI related to Section 4.1 for details) and C_D. We estimated A_{LR}, H_C, and A_C using plant-type

Table 2
Laboratory Experiments With Simulated Roots

Experiment set	1	2
Taproot diameter, D_T (m)	0.0019, 0.0059	0.0059
Taproot length, L_T (m)	0.18–0.45	0.175–0.45
GSD (Wet bulk density, ϕ)	Sand (1,467 kg/m^3, 35.9°), Gravel (1,522 kg/m^3, 52.2°), Mix (1,990 kg/m^3, 46.3°)	Sand (1,467 kg/m^3, 35.9°)
Taproot irregularities	With knots, Without knots	Without knots
Lateral root area, A_{LR} (cm^2)	0	3, 6, 12
Lateral root depth (m)	N/A	0.13–0.45
Lateral root diameter (m)	N/A	0.0015
Total number of experiments	108	40

specific regressions with D_S to eliminate the need for direct measurements of every seedling. We did not develop a regression for L_T given its large potential site-specific controls (e.g., groundwater, impermeable layer). We used new field measurements and previously published data to develop these allometric relations and to test F_P predictions.

2.2. Laboratory Experiments to Estimate *f*

We conducted laboratory experiments to test whether f varies with GSD, A_{LR}, root irregularities, and lateral root burial depth. Following previous studies (Schwarz et al., 2011), we used ropes to simulate roots to avoid root breakage and have repeatable conditions between experiments. In experiment Set 1, we used three different GSDs (well-sorted 1 mm diameter sand; gravel with sizes of 20–60 mm; mixture of 50% sand and 50% gravel) with moisture contents of 20% by weight (~28% by volume) to replicate conditions during field F_P measurements (Section 2.3.2). In half of the experiments, we tied 3 knots in the taproot to simulate taproot thickness irregularities (see Supporting Information S1). For each GSD and presence/absence of knots, we used two different D_T, each having 8–12 different values of L_T (Table 2).

In experiment Set 2, we used sand, a single D_T without knots, and simulated lateral roots sown into the taproot. Each lateral root had the same length and diameter to vary A_{LR} by changing the number of lateral roots. We varied the number of lateral roots (two, four, eight) or the lateral root depth (end of taproot, 10 cm above the end, combination of both depths; Figure S3 in Supporting Information S1) between experiments, with each of these conditions having a range of L_T.

We buried two (with lateral roots) or four (without lateral roots) taproots within a 27 cm diameter bucket. We held the taproots vertically during burial and placed them as far as possible from each other and the bucket walls. For the gravel and sand-gravel mix, the taproot did not remain perfectly vertical because large gravel particles leaned on it during filling. We observed similar taproot path deviations when excavating real roots in gravel (Section 2.3.2). Each lateral root was placed horizontally at the desired burial depth and was spread away from the other lateral roots. Although lateral roots may grow at any angle, we used horizontal roots to simplify data interpretation. After root placement, we vertically dropped the bucket 10 times from a height of 5 cm to settle the sediment.

We vertically pulled on each taproot using a load cell (Transducer Techniques MLP-300 with SSI display/logger) until the root was completely removed from the bucket and recorded the measured peak force as F_P. We measured ϕ by placing each GSD on a board, rotating the board until sediment started to move, and recording the angle at which movement occurred. We estimated the wet sediment bulk density as the wet sediment weight for a known volume. We back calculated f for each taproot using Equation 2 with the known F_P, D_T, L_T, λ, and ϕ. Therefore, we removed the effects of sediment friction angle, taproot diameter, and burial depth to isolate the effects of root-sediment friction, root irregularities, and lateral roots. We varied the sediment moisture content in a third experiment set (see Supporting Information S1) that verified our f values from Sets 1 and 2 were also

representative of the saturated bed conditions (Figure S4 in Supporting Information S1) that occur during high flows and seedling pullout.

2.3. Field Measurements of Allometric Scaling and F_P

2.3.1. Previously Published F_P and Seedling Characteristics

Bywater-Reyes et al. (2015) measured F_P, D_S, total root area, H_C, L_T, depth to groundwater, and A_C for *Populus, Salix*, and *Tamarix* seedlings grown at three different sites in the United States. They also manually scoured sediment around a test group of seedlings to explore how L_e affects F_P. The total root area was measured using scaled 2D photographs of excavated seedlings and included the taproot area. In their data, we estimated A_{LR} for each seedling as its total root area minus its average 2D taproot area ($0.5L_TD_S$), with any $A_{\mathrm{LR}}<0$ being removed from the data set. We developed allometric relations between $\log(D_S)$ and $\log(A_{\mathrm{LR}})$, $\log(H_C)$, and $\log(A_C)$ for all sites combined but separated *Populus/Salix* (native type) from *Tamarix* (invasive type). We compared our predicted and measured F_P (see SI for details on calculations) only in the Bitterroot (BR; mostly gravel, D_{50} = 23 mm) and Santa Maria (SM; mostly sand, D_{50} = 0.77 mm) Rivers because their GSDs were representative of our *f* experiments.

2.3.2. F_P and Seedling Characteristics on the Tagliamento River

Our study site focused on sand patches in a reach of the Tagliamento River, Italy (Latitude 46.235°N; Longitude 13.042°E; elevation 209.32 m a.s.l.) that has been previously used for analyses of riparian vegetation dynamics (e.g., Bertoldi & Gurnell, 2020). The dominantly gravel-bedded reach has an island-braided morphology with a braid plain up to 800 m wide and a longitudinal gradient of 0.0036 m/m. A sediment sample from our sand site had a 20% moisture content by weight, which set the moisture content in our *f* experiments (Section 2.2). The sieved GSD had a maximum size of 2 mm, and a median size of 0.1 mm with 11% of the distribution being finer than 0.044 mm.

We measured F_P for 20 seedlings that had finished one growing season at this sand site (D_S = 1.3–5.2 mm). For each seedling, we: (a) recorded the genus (*Populus* or *Salix*) and D_S, (b) attached a static cord to the seedling base and pulled vertically with the same load-cell winch system (Transducer Techniques MLP-300) as in Liffen et al. (2013) for large plants, or with a hand-held load cell (Wagner FDIX Force One) for small seedlings, (c) recorded the peak force as F_P, and (d) estimated L_T using scaled photos. We only predicted F_P (see details in SI) for five seedlings (four *Salix*, one *Populus*) because the remaining 16 experienced significant breakage.

We also excavated full root systems of 10 *Populus* and 10 *Salix* seedlings at the sand site to test whether allometric relations for *Populus*/*Salix* in the Tagliamento were similar to those from the United States' sites. For each excavated seedling, we measured D_S using calipers, H_C using rulers, and A_{LR} using scaled photographs. To partly validate Equation 3, we also measured D_T along z using scaled photos of three of these excavated seedlings (two *Populus*, one *Salix*; $L_T \sim$ 0.05–0.2 m) and using photos of three larger seedlings (two *Salix*, one *Populus*; $L_T \sim$ 0.4–0.6 m) excavated from other bars within the same reach.

3. Results

We first validated the general form of Equation 2 and explored controls of root irregularities, GSD, and A_{LR} on *f* using our laboratory measurements. We then used these data to develop a multiple regression equation for *f*. We next tested Equation 3 using our field measurements of D_T variation with z. We also developed allometric relations to predict A_{LR}, H_C, and A_C from D_S using the compiled field data, and used simple equations to estimate potential A_{LR} decline with sediment scour. With all necessary equations in place, we explored the sensitivity of the estimated F_P to controlling variables (e.g., GSD, irregularities). Finally, we compared predicted to measured F_P for the Tagliamento and United States' field sites.

3.1. Laboratory Experiments and Predictions of *f*

3.1.1. Measured Controls on F_P and *f*

In experiments without simulated lateral roots (Set 1), F_P increased with greater taproot 3D surface area for all tested L_T and D_T (Figure 2a) as expected from Equation 2. For a given total root surface area (3D taproot area +

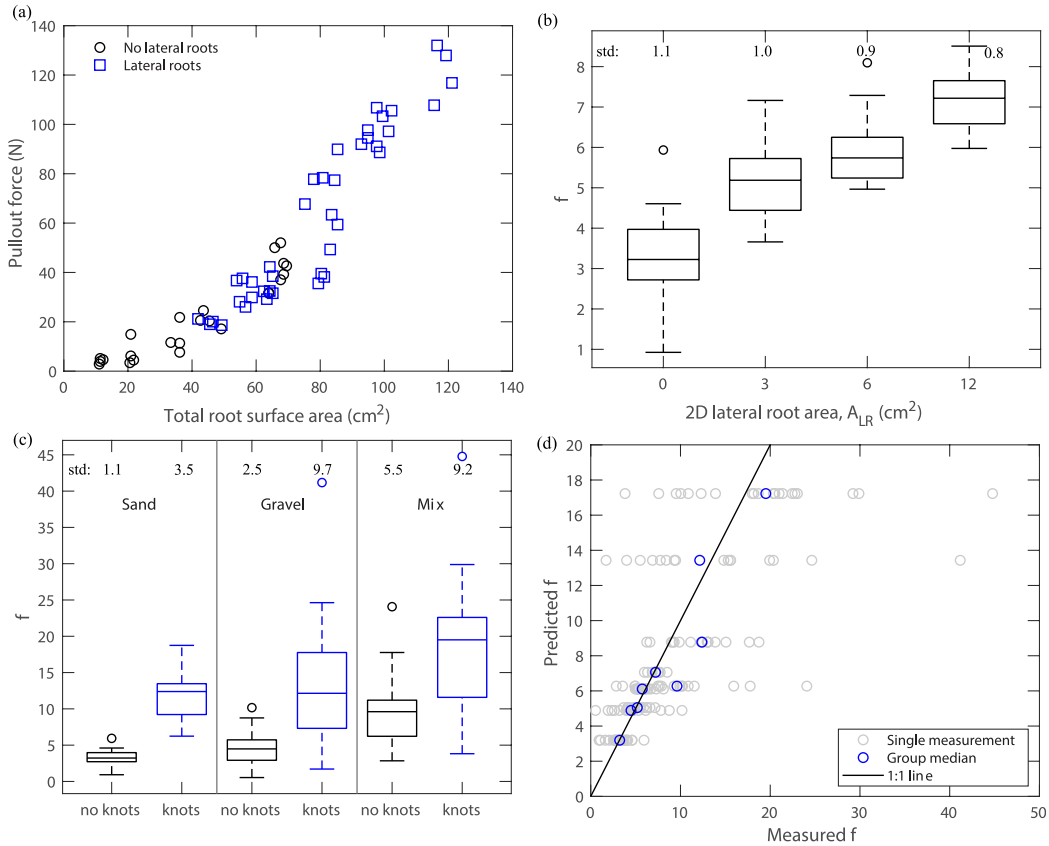

Figure 2. Experiments using buried ropes to simulate roots. (a) Measured pullout force (F_P) as a function of the total buried root surface area for knotless taproots buried in sand and that included or lacked lateral roots. (b) Measured root-sediment friction coefficient (f) distributions for different 2D lateral root areas (A_{LR}) for knotless roots buried in sand. Std is the standard deviation of each distribution. (c) Measured f distributions for taproots without lateral roots as a function of different GSD and presence/absence of knots. (d) Predicted (Equation 12) versus measured f for every experiment (gray) with median values (blue) for grouped experimental conditions (A_{LR}, presence/absence of knots, GSD).

3D lateral root area), experiments with (Set 2) and without lateral roots generally had the same measured F_P (Figure 2a). Lateral root burial depth also did not affect F_P (Figure S2 in Supporting Information S1). Lateral roots therefore simply enhanced root-sediment friction (f) through added root areas and did not impact the total overlying sediment weight resisting root pullout. We conclude that lateral root effects can just be included in f without needing detailed lateral root architecture information in Equation 2. Note that all taproot areas throughout this paper are 3D surface areas and the added lateral root areas in Figure 2a are also 3D surface areas. All other reported lateral root areas (A_{LR}) for laboratory experiments, equations, and field measurements are 2D planar areas to be consistent with field A_{LR} being derived from 2D photographs. We isolated lateral root impacts on f by calculating the median f for a given A_{LR} in experiment Set 2 (sand, without knots). Median f increased with greater A_{LR}, which further confirmed that lateral root area partly controls root-sediment friction (Figure 2b).

Experiments without lateral roots (Set 1) showed that GSD and knots also control f. Holding the presence/absence of knots constant, median f increased from sand to gravel to mixed sediment, implying that f is greater with coarser/wider GSD (Figure 2c). We controlled for differences in sediment bulk density and friction angle between GSDs when estimating f; the GSD has additional impacts on f beyond these commonly used variables. The standard deviation (std) of the f distribution also increased with coarser/wider GSD. For a given GSD, high f likely occurred when large grains directly on top of (or adjacent to) the taproot pinched the taproot and needed to be displaced before the taproot could be removed. When not in contact with the taproot, such large rocks had little to no effect, producing low f values for both the gravel and sediment mixture that were similar to those for sand. We observed a similar process during field seedling excavation; taproots were difficult to remove if overlain or wedged by large gravel or cobbles. In addition to these large grain effects, the median and standard deviation of f

were the largest for the sediment mixture likely because sand filled gravel pore spaces, thereby increasing local root-sediment contact areas. Taproot knots also increased the median f and the standard deviation in the f distribution (Figure 2c) for a given GSD. Knots acted in a similar way to large grains; the taproot would be temporarily stuck during pullout as knots interacted with surrounding particles, particularly large rocks.

3.1.2. Equation to Predict f

In our experiments, f was generally at least an order of magnitude larger than those previously used (e.g., 0.7–0.9) (Calvani et al., 2019) to predict F_P (Figures 2b and 2c). We concluded that a new equation was needed for f for gravel-bedded rivers. We first developed a multiple regression between $\log(f)$ and log transformed nominal metrics for GSD (sand = 1, gravel = 2, mix = 3) and knots (without knots = 1, with knots = 2) using all experiments without lateral roots (Set 1)

$$f = 10^{0.50+0.61\ \log(\mathrm{GSD})+1.46\ \log(\mathrm{knots})}, R^2 = 0.72, \text{adj. } R^2 = 0.52, p < 1 \times 10^{-5} \tag{11}$$

We then initially developed a linear regression between f and A_{LR} for the experiments with lateral roots (Set 2). However, this predicted unrealistic values of f (e.g., 1×10^6) for field seedlings with A_{LR} much greater than those tested in the lab and demonstrated that f does not steadily increase with A_{LR}. We therefore fit an exponential function that: (a) asymptotes to a constant value of f for $A_{\mathrm{LR}} > 12$ cm^2 (maximum value in lab) and (b) predicts f equal to that from Equation 11 when $A_{\mathrm{LR}} = 0$ (knotless taproot in sand) to seamlessly combine the two regressions.

$$f = 10^{0.50+0.61\ \log(GSD)+1.46\ \log(\mathrm{knots})} + 4.33\left(1 - e^{(-1866 A_{\mathrm{LR}}(L_e))}\right) \tag{12}$$

The second term on the right side of Equation 12 is from the second regression ($R^2 = 0.68$, $p < 0.003$), where $A_{\mathrm{LR}}(L_e)$ is the area of lateral roots remaining for a given scour depth. We lacked sediment scour in our experiments and $A_{\mathrm{LR}}(L_e) = A_{\mathrm{LR}}$, but in the field, scour will decrease lateral root area and f (see Section 3.3). The median predicted f from Equation 12 closely matched the median measured f for a given experimental condition (i.e., A_{LR}, GSD, knots) (Figure 2d), as expected. Equation 12 only predicts a single f for a given condition and cannot capture measured f variability (std) that was driven by local sediment packing or large rocks. Uncertainties in f predictions are therefore likely to be an important source of F_P prediction uncertainties (see Section 3.5). Future work is also needed on f values for seedlings with A_{LR} larger than 12 cm^2.

3.2. Validation of D_{T} Variation With z

We tested whether D_T decreases with vertical distance belowground as predicted by Equation 3 or remains constant as assumed in previous studies. Despite careful efforts, no taproot was excavated to its full length and smallest diameter because of the delicacy of small roots. For example, our smallest measured D_T was relatively large ($0.15–0.37 D_S$) because the taproot broke. We therefore estimated L_T for each seedling using the measured D_S in Equation 3; we forced D_T at the taproot end to equal the predicted value. Equation 3 predicted the general measured D_T decline with z for the tested seedlings (Figure 3), indicating that assuming a constant D_T is likely incorrect. Random D_T variations were superimposed on this general vertical decline in D_T and could be partly caused by photo measurement error. However, visual inspection of real taproots showed that large D_T fluctuations are driven by root shape irregularities (thigmotropism) and further confirmed the potential field importance of "knots" used in our laboratory measurements of f. Such random D_T variations, which are not represented by Equation 3, likely add significant uncertainties to F_P predictions in addition to the f spatial variations that are not captured by Equation 12.

3.3. Allometric Relations and A_{LR} Decrease With Scour

For a given seedling, we require A_{LR} to calculate F_P and require H_C and A_C to determine F_D and L_c. We used data from Bywater-Reyes et al. (2015) to develop regressions between these variables and D_S (Figure S5 in Supporting Information S1) for *Populus/Salix* and *Tamarix*

$$\log(H_C) = 1.49 + 0.91 \log(D_S) \text{ for Populus/Salix, } R^2 = 0.55,\ p < 0.0001 \tag{13-1}$$

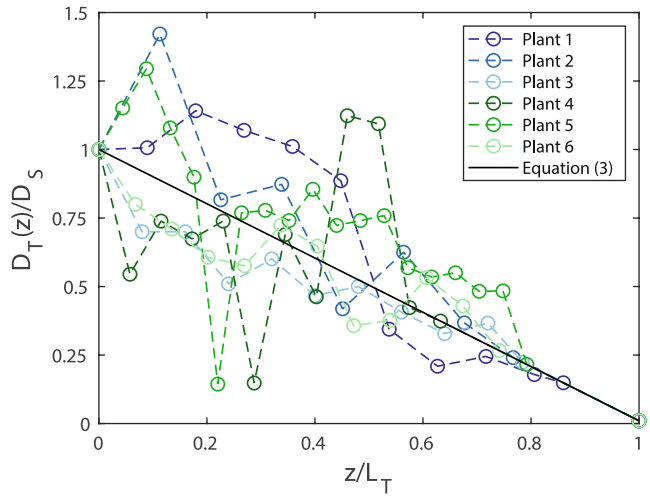

Figure 3. Measured normalized taproot diameter ($D_T(z)/D_S$) as a function of normalized vertical distance (z/L_T) for six seedlings. Equation 3 is the solid black line.

$$\log(H_C) = 0.61 + 0.36\log(D_S) \text{ for Tamarix, } R^2 = 0.40,\ p < 0.0001 \quad (13\text{-}2)$$

$$\log(A_C) = 1.94 + 1.82\log(D_S) \text{ for Populus/Salix, } R^2 = 0.75,\ p < 0.0001 \quad (14\text{-}1)$$

$$\log(A_C) = 0.03 + 0.99\log(D_S) \text{ for Tamarix, } R^2 = 0.59\ (p = 0.9 \text{ intercept},\ p < 0.0001 \text{ slope}) \quad (14\text{-}2)$$

$$\log(A_{\mathrm{LR}}) = 0.80 + 1.57\log(D_S) \text{ for Populus/Salix, } R^2 = 0.54,\ p < 0.06 \quad (15\text{-}1)$$

$$\log(A_{\mathrm{LR}}) = -1.54 + 0.46\log(D_S) \text{ for Tamarix, } R^2 = 0.20,\ p < 0.04 \quad (15\text{-}2)$$

We tested multiple regression equations that also included distance to groundwater, but only H_C for *Tamarix* had a statistically significant ($p < 0.1$) influence from groundwater and we therefore ignored the groundwater effects discussed by Bywater-Reyes et al. (2015). Measured A_{LR} and H_C for *Populus/Salix* in the Tagliamento River were within the *Populus/Salix* data scatter from Bywater-Reyes et al. (2015) (Figure S5 in Supporting Information S1). Although likely important, site-specific controls (e.g., groundwater depth, solar exposure) on these allometric scaling relations could not be isolated and we used Equations 13-1, 13-2, 15-1, and 15-2 for all subsequent calculations.

While Equation 15 predicts lateral root area before any scour, another equation is necessary to estimate the remaining lateral root area for a given scour depth ($A_{LR}(L_e)$). Vertical A_{LR} distributions are not generally quantified for *Salix, Populus*, or *Tamarix*. Based on similar assumed equation forms as in Cunico et al. (2024), we therefore assumed three different possible root distributions where A_{LR} is: (a) linearly distributed throughout L_T ($b = 1$), (b) concentrated near the surface ($b = 7$), or 3) concentrated at depth ($b = 0.15$). We estimated $A_{\mathrm{LR}}(L_e)$ for these three conditions (Figure 4) using the different listed exponents (b) in

$$A_{\mathrm{LR}}(L_e) = A_{\mathrm{LR}}\left[1 - \frac{L_e}{L_T}\right]^b \quad (16)$$

3.4. Predicted Controls on F_P

With all equations developed, we explored F_P sensitivity to D_S, GSD (sand vs. mixture), root shape irregularities (knots in our experiments), and root hairs. We used Equations 2 and 3, 12, 15-1, and 15-2 for *Populus/Salix*, (16) with $b = 1$, and the following values: ϕ from Table 2, $\lambda = 0.3$, $\rho_s = 2{,}650$ kg/m^3, $\rho = 1{,}000$ kg/m^3, $L_e = 0$ m, and $L_T = 0.3$ m. As expected, F_P increased with larger D_S because of greater taproot and lateral root areas associated with larger seedlings (Figures 5a and 5b). For the same D_S, F_P was 2–2.7 times higher for seedlings in a sediment

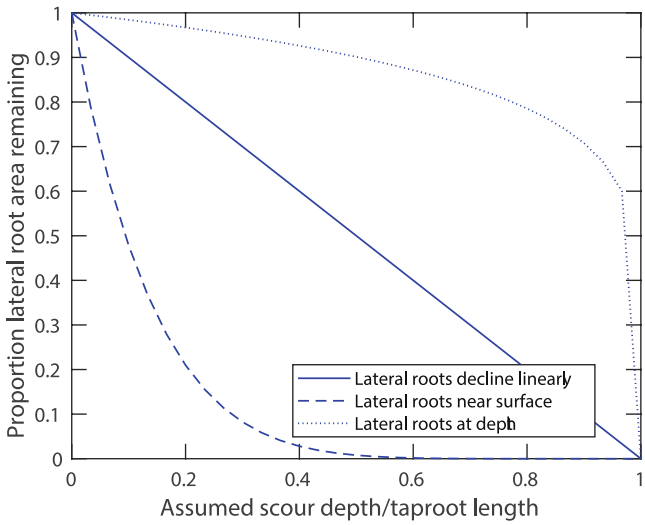

Figure 4. Effect of normalized scour depth (L_e/L_T) on the proportion of lateral root area remaining buried ($A_{LR}(L_e)/A_{LR}$) for three different assumed vertical distributions of A_{LR}.

mixture than in pure sand because of higher f and ϕ for the sediment mixture (Figure 5a vs. 5b). Holding all else constant, addition of root shape irregularities or hairs increased F_P by a factor of 1.7–2.6 or 2.2, respectively, and including both effects resulted in 3.8–5.8 times higher F_P. Root shape irregularities had greater impacts on F_P for the sediment mixture than for sand, reflecting measured f changes with knots for different sediments in our experiments (Figure 2c). In summary, ignoring the effects of coarse GSDs, root shape irregularities, and root hairs can result in large underestimates of F_P.

We now examine how L_e affects F_P using the three different potential $A_{LR}(L_e)$ forms resulting from Equation 16 and by unrealistically assuming A_{LR} is unaffected by scour. To generalize our results, we discuss normalized scour depths (L_e/L_T) and pullout forces ($F_P(L_e)/F_P(L_e = 0)$), where the normalized pullout forces are pullout forces for a given scour depth divided by the pullout force without any scour. Irrespective of input variables, F_P was generally ~35%-50% or 5%–10% of its pre-scour value when the scour depth was 20% or 50%, respectively, of the taproot length (Figures 5c and 5d). This implies that a relatively small amount of scour can significantly reduce the root resistance force keeping seedlings in place and therefore the fluid force needed to remove seedlings.

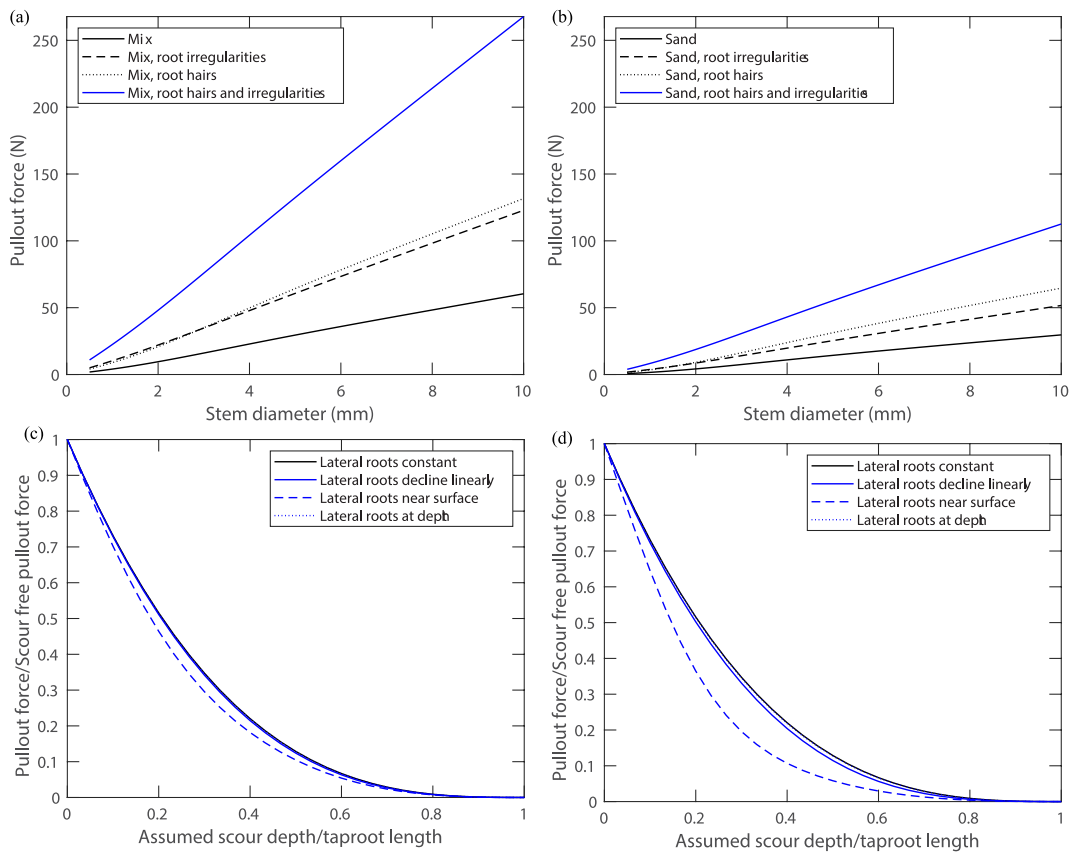

Figure 5. Effects of stem diameter, root shape irregularities, and root hairs on predicted F_P for (a) a sediment mixture and (b) sand. (c, d): Effect of L_e/L_T on normalized pullout forces for different lateral root distributions (Equation 16, blue lines) or for assuming lateral roots do not change with scour (black line). (c) Calculations are for a high total friction from a sediment mixture with root irregularities and hairs versus (d) a low total friction from sand with no root irregularities or hairs. Any lines not visible in (c, d) are underneath other lines.

The relation between normalized pullout forces and scour depths was independent of D_S and L_T and only depended on frictional sources (GSD, root irregularities, root hairs, A_{LR}) (Figures 5c and 5d). The assumed vertical distribution of A_{LR} had little influence on normalized pullout forces when total friction was high (i.e., root irregularities, root hairs, sediment mix) (Figure 5c) but a relatively large impact when total friction was small (i.e., no root irregularities, no root hairs, sand) (Figure 5d). This occurred because the proportional influence of A_{LR} on f, compared to all other frictional sources, changes with total friction (see Figure 2c). For low total friction, A_{LR} has a relatively high proportional influence on f, causing different lateral root distributions to change the normalized pullout force by up to 50%.

Regardless of total friction, the vertical A_{LR} distribution had the largest impact on normalized pullout forces at intermediate L_e/L_T (~0.2–0.6) because of competing effects as L_e/L_T increased. For example, when scour depths are small ($L_e/L_T < 0.2$), small changes in f because of low lateral root loss are multiplied by large overlying sediment weights and large taproot areas (Equation 2) to have little impact on F_P. At large scour depths ($L_e/L_T > 0.6$), large changes in f from high lateral root loss are multiplied by small overlying sediment weights and small taproot areas to also cause little change in F_P. Instead, moderate scour depths have significant changes in f multiplied by moderate overlying sediment weights and taproot areas to cause large F_P changes.

3.5. Field Validation of Predicted F_P

We used field measured F_P (Section 2.3) to test: (a) our predictions of F_P using Equations 2 and 3, 12, 15-1, 15-2, and 16, (b) the importance of root hairs by removing their effect from Equations 2, and 3) the importance of a vertically changing D_T by assuming $D_T(z) = D_S$ instead of using Equation 3. Details on the input variables used for each site are provided in the Supporting Information S1. We compared the predicted and measured F_P using the log-transformed mean-absolute error (MAE) (see Yager et al., 2012 for details).

Assuming a constant $D_T(z)$ resulted in systematic over-prediction of F_P (MAE = 3.8) with 78% of observations being over-predicted and 19% being over-predicted by more than an order of magnitude (Figure 6a). This occurred because constant $D_T(z)$ multiplies the large overlying sediment weights at the taproot bottom by incorrectly high taproot areas. Removal of root hair effects counteracted the constant $D_T(z)$ to improve F_P predictions (MAE = 3.0) (Figure 6b). In previous studies, constant $D_T(z)$ may have produced accurate F_P or L_c predictions because root hair effects were excluded and low f values were employed (0.7–0.9) (Calvani et al., 2019). We suggest instead that F_P predictions include $D_T(z)$ variations because our measured $D_T(z)$ declined with z, even for small seedlings (Figure 3).

With $D_T(z)$ represented by Equation 3, accurate F_P predictions were only obtained by including root hair effects. Excluding root hair effects resulted in systematic under-prediction of F_P (84% of data; 15% by more than an order of magnitude) and high prediction errors (MAE = 4.3) (Figure 6d). Including root hairs provided the lowest observed prediction errors (MAE = 2.9) without systematic under- or over-prediction (Figure 6c). Prediction accuracy was independent of both plant type (*Populus/Salix* vs. *Tamarix*) and manually imposed scour depths, implying that the combination of Equations 2 and 3, 12, 15-1, 15-2, and 16 generally captured these two effects on F_P. Systematic under-prediction of F_P at all sand sites occurred because these locations likely had silt/clay material that had cohesive effects, which were neglected in our calculations.

Even with root hair and $D_T(z)$ variation effects included in Equation 2, F_P prediction errors were up to an order of magnitude (Figure 6c). Such errors partly occurred because of large uncertainties in A_{LR} estimated from Equations 15-1 and 15-2; A_{LR} had an order of magnitude of scatter for a given D_S (Figure S5 in Supporting Information S1). However, F_P predictions were relatively insensitive to A_{LR} if other significant frictional sources were present (e.g., gravel, root irregularities) (Figure 5c), which occurred for all sites. Therefore, F_P prediction errors were most likely caused by unaccounted for local field variations in f given the high f variability measured for a given laboratory condition (Figure 2). Further uncertainties may have resulted from unquantified spatial variability in λ, $D_T(z)$, ϕ, and bed saturation as well as from unquantified matrix suction effects (see Supporting Information S1).

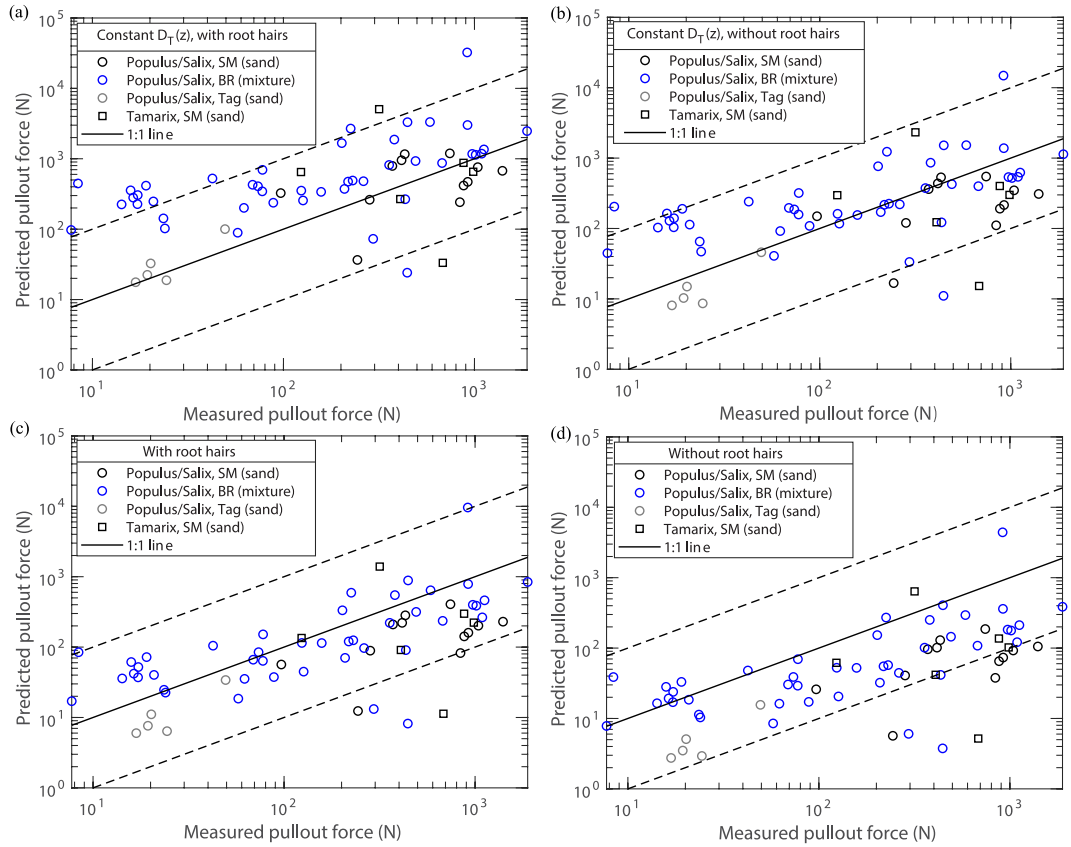

Figure 6. Measured versus predicted F_P for the Bitterroot (BR) and Santa Maria Rivers (SM) from Bywater-Reyes et al. (2015) and for the Tagliamento River (Tag). *Populus/Salix* (circles), *Tamarix* (squares), sand sites (black and gray), and sediment mixtures (blue) are shown with a 1:1 line (solid black) and order of magnitude of prediction uncertainty (dashed black lines). In (a, b) a vertically constant taproot diameter is employed whereas in (c, d) the taproot diameter changes as shown in Figure 3 (Equation 3). Predictions in (a, c) include root hairs, whereas those in (b, d) exclude root hairs.

4. Discussion

Accurate pullout force predictions are required: (a) friction coefficients that account for GSD, root irregularities, and lateral roots, (b) decreases in taproot diameter with vertical distance belowground, and (c) root hair effects. Specifically, friction coefficients developed from pulling metal rods through soil (Calvani et al., 2019; Potyondy, 1961) were at least an order of magnitude smaller than what we measured for coarse alluvial sediments (Figure 2) and resulted in underpredictions of F_P by orders of magnitude. Root-sediment friction in rivers therefore cannot be accurately estimated from agricultural or construction studies that use much finer sediment. However, we observed considerable scatter in the friction coefficient for a given sediment and root condition (Figure 2). Estimates of root-sediment friction could be improved through future experiments. For example, we co-varied the GSD variance and median size in our experiments and could not separate these two effects. We suggest additional experiments to further improve our f equation that: (a) independently vary GSD moments, (b) have a wider range of lateral root depths, areas, and angles, and (c) include lateral root irregularities.

We developed F_P and scour depth predictions using allometric relations for *Populus/Salix* and *Tamarix* but similar predictions could be expanded to other species/plant types by simply replacing these scaling relations in Equations 13-1, 13-2, 14-1, 14-2, 15-1, and 15-2. Further, we observed root hairs when excavating *Populus/Salix* but for any plants lacking root hairs, the root hair correction factor could be simply set to zero. Although we ignored the effects of pronation angle in both our measured and predicted F_P, our F_P predictions for manually pronated seedlings from Bywater-Reyes et al. (2015) still reasonably match the measured values. Development of predictive equations for pronation angles could improve future F_P estimates. We only account for root pullout resistance to seedling removal, but seedlings could instead be removed by taproot breakage if the flow strength

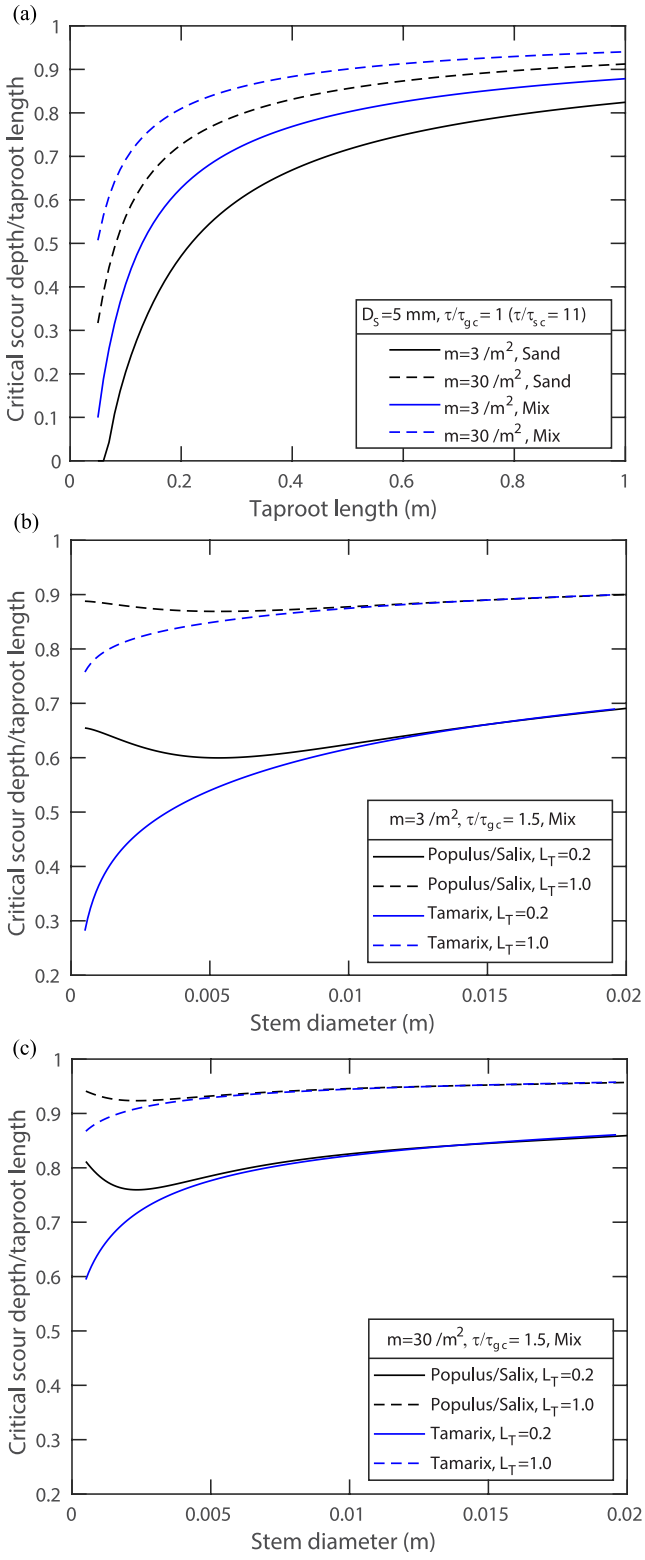

Figure 7. (a) Critical scour depth (L_c/L_T) variation with taproot length (L_T), plant density (m), and sediment type (sand vs. sediment mixture). Critical scour depth variation with D_T, L_T, and plant type for a sediment mixture with m of (b) 3 m^{-2} or (c) 30 m^{-2}.

exceeds the root tensile strength. Future work on a root breakage equation would provide a comprehensive understanding of the effects of scour depth on seedling removal.

4.1. Implications for Channel Morphodynamics and Restoration of Native Species

In morphodynamic or riparian vegetation recruitment models, thresholds for physical disturbance and seedling removal by the flow include a critical Shields number, critical proportion of belowground biomass that is scoured, or critical bed erosion depth (Benjankar et al., 2020; Bertoldi et al., 2014; Caponi & Siviglia, 2018; Li et al., 2022; Tranmer et al., 2023). Such thresholds are usually assumed to be independent of vegetation characteristics, which may not be physically reasonable. For example, previous studies have found that the critical scour depth for seedling removal should vary with total root biomass, length or volume, taproot depth, and/or the vertical root distribution (Caponi & Siviglia, 2018; Taye et al., 2026). To test if other variables are important, we predicted the relative critical scour depth needed for seedling removal (L_c/L_T) using Equations 2–10, (12), (13–15) for *Populus/Salix* seedlings, and (16) with assumed values for the GSD, L_T, D_S, C_P, C_D, and plant density within a patch (m). We iteratively solved this system of equations using reach-averaged flow conditions capable of transporting gravel ($\tau/\tau_{cg} = 1$; τ = reach-averaged shear stress, τ_{cg} = critical shear stress for gravel) and calculated the corresponding transport stage for sand (τ/τ_{cs}) for the same τ (see Supporting Information S1 for details).

For a given τ, relative critical scour depths varied substantially (e.g., 0.1–0.9) with GSD and vegetation density (Figure 7). Holding all else constant, seedlings in sand required lower L_c/L_T than those growing in sediment mixtures (Figure 7a) because of lower root-sediment friction. Seedlings in dense vegetation patches (high m) required greater L_c/L_T than those in sparse patches (low m) (Figure 7a) because they experienced lower flow velocities and therefore drag forces. The critical scour depth also varied with reach-averaged flow conditions and aboveground seedling characteristics (discussed below). Assuming a constant critical scour depth in morphodynamic models could result in large errors in predicted vegetation removal and resulting flow, sediment transport, and morphology changes. Explicit implementation of our proposed equations in reach-scale morphodynamic models would likely require significant computational time and large amounts of input variable information that may prove prohibitive. Instead, our estimated variability in critical scour depths could be implemented in such models using statistical approaches (Cunico et al., 2024) to investigate how critical scour depths influence morphodynamic changes.

Our calculations also have implications for riparian vegetation restoration. For example, L_c/L_T strongly varied with taproot length when $L_T \leq 0.3$ m (Figure 7a). Therefore, seedlings with taproot lengths limited by high water tables or by growth in the channel near baseflow elevation (Broadfoot, 1973; Cooper et al., 1999; Mahoney & Rood, 1992; Naumburg et al., 2005; Scott et al., 1996; Stromberg et al., 2007; Tron et al., 2014) may be particularly susceptible to scour. Seedlings growing in dense vegetation patches required relatively high L_c/L_T (Figure 7a) and such patches may also experience lower sediment scour depths than sparse patches for the same upstream sediment supply (Yager & Schmeeckle, 2013). Thus, seedlings in dense patches could

be more scour stable than those in sparse patches. Restoration of *Populus/Salix* through seeding planting programs may benefit from denser plantings with appropriate groundwater levels to reduce seedling removal through scour. Conversely, dense plantings may result in greater competition and less healthy seedlings (Adair & Binkley, 2002; Tozzi et al., 2013). A holistic understanding of seedling density effects on competition, applied fluid forces, and F_P may inform the best planting density.

4.2. Removal of Native Versus Invasive Species by Scour

Some restoration efforts include manual or flow-driven removal of non-native plants (e.g., *Tamarix* in the United States) (González et al., 2017; Kui et al., 2019; Shafroth et al., 2010; Stromberg et al., 2007) or sometimes even native species that have stabilized normally bare channel bars that provide critical avian habitat (Johnson, 1997). We compared predicted L_c/L_T for different aged *Populus/Salix* and *Tamarix* seedlings growing in a sediment mixture and subjected to $\tau/\tau_{cg} = 1.5$ (see SI for details). We assumed D_S was a proxy for age and that L_T was independent of D_S and was limited by external factors (e.g., groundwater level).

For *Populus/Salix*, L_c/L_T was mostly independent of seedling age for low m (Figure 7b) and counterintuitively was greater for younger plants (smaller D_S) than older plants for large m (Figure 7c). In contrast, *Tamarix* required greater L_c/L_T for older seedlings (larger D_S) regardless of m. *Tamarix* also required lower L_c/L_T than *Populus/Salix* for young seedlings (e.g., $D_S < 5$ mm), implying that young *Tamarix* may be more susceptible to flow removal than *Populus/Salix*. Older invasive seedlings (e.g., $D_S > 10$ mm) had similar removal potential as native plants. These results demonstrate that *Tamarix* removal throughflow releases could likely only occur when seedlings are very small (~ first year of growth), as empirically demonstrated by Bywater-Reyes et al. (2015). Manual removal could be required for older *Tamarix* to avoid also scouring *Populus/Salix* of similar sizes. We conclude that *Tamarix* scour resistance is not a major contributor to *Tamarix* outcompeting *Populus/Salix* in regulated United States' streams. Instead, *Tamarix* has different drought and salt tolerances, adaption to disturbances, or tolerance of high/low nutrient levels (Edwards, 2024; Edwards et al., 2024).

Predicted L_c/L_T differences between *Tamarix* and *Populus/Salix* were controlled by the allometric relations for A_{LR}, H_C, and A_C for each plant type (Equations 13-1, 13-2, 14-1, 14-2 15-1, and 15-2 and Figure S5 in Supporting Information S1). For low D_S, *Tamarix* had both higher canopy areas (A_C) and greater canopy heights (H_C) than *Populus/Salix*, causing higher applied flow velocities and drag forces and therefore lower required L_c/L_T. For large D_S, *Tamarix* had slightly higher H_C but lower A_C compared to *Populus/Salix*, resulting in similar L_c/L_T. For *Populus/Salix*, minimum L_c/L_T values occurred at moderate D_S because of similar allometric tradeoffs between A_{LR}, H_C, and A_C with larger D_S. A better understanding of the site-specific controls (e.g., depth to groundwater, climate) on these allometric relations (Bywater-Reyes et al., 2015) could improve L_c/L_T predictions for invasive and native species.

5. Conclusions

We presented a new mechanistic equation for the pullout force resisting riparian seedling removal by the flow. Our equation incorporates root-sediment friction, root hair effects, taproot diameter changes with vertical distance belowground, and sediment scour effects on remaining root areas. Laboratory experiments demonstrated that previously employed constant root-sediment friction coefficients could be orders of magnitude too low. We instead developed an empirical equation for root-sediment friction varying with the bed grain size distribution, root irregularities, and lateral root areas. Predicted pullout forces matched measured values only if we incorporated these frictional effects, root hairs, and taproot diameter changes with depth.

We combined our pullout force equation with equations for the applied fluid force on an individual seedling within a vegetation patch to determine the critical scour depth for seedling removal by the flow. Contrary to common assumptions in morphodynamic models, the critical scour depth was not constant and should be treated as a dynamic parameter influenced by belowground and aboveground seedling traits, reach-averaged flow conditions, bed grain size distributions, and vegetation density. Invasive and native seedlings had similar critical scour depths except for very young plants, which suggests that invasive species removal strategies (i.e., flow based vs. manual) should vary with seedling age.

Conflict of Interest

The authors declare no conflicts of interest relevant to this study.

Availability Statement

All new field and laboratory measurements are available in a Mendeley Data repository (Yager, 2026) directly accessible at https://data.mendeley.com/datasets/nv8d639cv9/1. Field measurements from other studies are published as part of those studies and are not included in our published data.

Acknowledgments
Funding was provided by a Fulbright Foundation Research Scholar grant to EMY and by a grant from the European Union under NextGenerationEU, to the project Green Rivers, PRIN 2022 PNRR Prot. n. 407 P20229WTX7 to WB. We thank Aina Barcelona and Angela Gurnell for help with field data collection. The authors thank the Associate Editor Andrew Wilcox, Sharon Bywater-Reyes and two anonymous reviewers for their constructive comments and suggestions. Open access publishing facilitated by Universita degli Studi di Trento, as part of the Wiley - CRUI-CARE agreement.

References

Adair, E. C., & Binkley, D. (2002). Co-limitation of first year Fremont cottonwood seedlings by nitrogen and water. *Wetlands*, *22*(2), 425–429. https://doi.org/10.1672/0277-5212(2002)022[0425:clofyf]2.0.co;2

Bailey, P. H. J., Currey, J. D., & Fitter, A. H. (2002). The role of root system architecture and root hairs in promoting anchorage against uprooting forces in Allium cepa and root mutants of Arabidopsis thaliana. *Journal of Experimental Botany*, *53*(367), 333–340. https://doi.org/10.1093/jexbot/53.367.333

Bau', V., Zen, S., Calvani, G., & Perona, P. (2019). Extracting the critical rooting length in plant uprooting by flow from pullout experiments. *Water Resources Research*, *55*(12), 10424–10442. https://doi.org/10.1029/2019WR025074

Belote, R. T., Makarick, L. J., Kearsley, M. J. C., & Lauver, C. L. (2010). Tamarisk removal in Grand canyon national Park: Changing the native-non-native relationship as a restoration goal. *Ecological Restoration*, *28*(4), 449–459. https://doi.org/10.3368/er.28.4.449

Benjankar, R., Tranmer, A. W., Vidergar, D., & Tonina, D. (2020). Riparian vegetation model to predict seedling recruitment and restoration alternatives. *Journal of Environmental Management*, *276*, 111339. https://doi.org/10.1016/j.jenvman.2020.111339

Bertoldi, W., & Gurnell, A. M. (2020). Physical engineering of an island-braided river by two riparian tree species: Evidence from aerial images and airborne lidar. *River Research and Applications*, *36*(7), 1183–1201. https://doi.org/10.1002/rra.3657

Bertoldi, W., Siviglia, A., Tettamanti, S., Toffolon, M., Vetsch, D., & Francalanci, S. (2014). Modeling vegetation controls on fluvial morphological trajectories. *Geophysical Research Letters*, *41*(20), 7167–7175. https://doi.org/10.1002/2014GL061666

Boothroyd, R. J., Hardy, R. J., Warburton, J., & Marjoribanks, T. I. (2016). The importance of accurately representing submerged vegetation morphology in the numerical prediction of complex river flow. *Earth Surface Processes and Landforms*, *41*(4), 567–576. https://doi.org/10.1002/esp.3871

Bouma, T. J., van Duren, L. A., Temmerman, S., Claverie, T., Blanco-Garcia, A., Ysebaert, T., & Herman, P. M. J. (2007). Spatial flow and sedimentation patterns within patches of epibenthic structures: Combining field, flume and modelling experiments. *Continental Shelf Research*, *27*(8), 1020–1045. https://doi.org/10.1016/j.csr.2005.12.019

Braatne, J., Rood, S., & Heilman, P. (1996). Life history, ecology and reproduction of riparian cottonwoods in North America. In *Biology of populus and its implications for management and conservation* (pp. 57–85). NRC Research Press.

Broadfoot, M. W. (1973). *Water table depth and growth of young cottonwood*. USDA-Forest Service, Southern Forest Experiment Station.

Bywater-Reyes, S., Wilcox, A. C., & Diehl, R. M. (2017). Multiscale influence of woody riparian vegetation on fluvial topography quantified with ground-based and airborne lidar. *Journal of Geophysical Research: Earth Surface*, *122*(6), 1218–1235. https://doi.org/10.1002/2016JF004058

Bywater-Reyes, S., Wilcox, A. C., Stella, J. C., & Lightbody, A. F. (2015). Flow and scour constraints on uprooting of pioneer woody seedlings. *Water Resources Research*, *51*(11), 9190–9206. https://doi.org/10.1002/2014WR016641

Cai, G., & Ahmed, M. A. (2022). The role of root hairs in water uptake: Recent advances and future perspectives. *Journal of Experimental Botany*, *73*(11), 3330–3338. https://doi.org/10.1093/jxb/erac114

Calvani, G., Francalanci, S., & Solari, L. (2019). A physical model for the uprooting of flexible vegetation on River bars. *Journal of Geophysical Research: Earth Surface*, *124*(4), 1018–1034. https://doi.org/10.1029/2018JF004747

Caponi, F., Koch, A., Bertoldi, W., Vetsch, D. F., & Siviglia, A. (2019). When does vegetation establish on gravel bars? Observations and modeling in the alpine Rhine River. *Frontiers in Environmental Science*, *7*, 124. https://doi.org/10.3389/fenvs.2019.00124

Caponi, F., & Siviglia, A. (2018). Numerical modeling of plant root controls on gravel bed River morphodynamics. *Geophysical Research Letters*, *45*(17), 9013–9023. https://doi.org/10.1029/2018GL078696

Chen, Z., Ortiz, A., Zong, L., & Nepf, H. (2012). The wake structure behind a porous obstruction and its implications for deposition near a finite patch of emergent vegetation. *Water Resources Research*, *48*(9), 2012WR012224. https://doi.org/10.1029/2012WR012224

Cooper, D. J., Merritt, D. M., Andersen, D. C., & Chimner, R. A. (1999). Factors controlling the establishment of Fremont cottonwood seedlings on the Upper Green River, USA. *Regulated Rivers: Research & Management*, *15*(5), 419–440. https://doi.org/10.1002/(sici)1099-1646(199909/10)15:5<419::aid-rrr555>3.0.co;2-y

Corenblit, D., Vidal, V., Cabanis, M., Steiger, J., Garófano-Gómez, V., Garreau, A., et al. (2016). Seed retention by pioneer trees enhances plant diversity resilience on gravel bars: Observations from the river Allier, France. *Advances in Water Resources*, *93*, 182–192. https://doi.org/10.1016/j.advwatres.2016.02.015

Cunico, I., Bertoldi, W., Caponi, F., Dijkstra, H. A., & Siviglia, A. (2024). River ecomorphodynamic models exhibit features of nonlinear dynamics and chaos. *Geophysical Research Letters*, *51*(11), e2023GL107951. https://doi.org/10.1029/2023GL107951

Curran, J. C., & Hession, W. C. (2013). Vegetative impacts on hydraulics and sediment processes across the fluvial system. *Journal of Hydrology*, *505*, 364–376. https://doi.org/10.1016/j.jhydrol.2013.10.013

De Baets, S., Denbigh, T. D. G., Smyth, K. M., Eldridge, B. M., Weldon, L., Higgins, B., et al. (2020). Micro-scale interactions between Arabidopsis root hairs and soil particles influence soil erosion. *Communications Biology*, *3*(1), 164. https://doi.org/10.1038/s42003-020-0886-4

Defina, A., & Bixio, A. C. (2005). Mean flow and turbulence in vegetated open channel flow. *Water Resources Research*, *41*(7), 2004WR003475. https://doi.org/10.1029/2004WR003475

Edmaier, K., Crouzy, B., & Perona, P. (2015). Experimental characterization of vegetation uprooting by flow. *Journal of Geophysical Research: Biogeosciences*, *120*(9), 1812–1824. https://doi.org/10.1002/2014JG002898

Edwards, P. J. (2024). Ecological traits of Saliceae and the species replacing them on the active floodplain. *River Research and Applications*, *40*(6), 988–1000. https://doi.org/10.1002/rra.4229

Edwards, P. J., Hügli, C., Olde Venterink, H., & Ramseier, D. (2024). Phosphorus enrichment enabled Amorpha fruticosa to invade on the floodplain of the Tagliamento River, Italy. *Biological Invasions*, *26*(1), 201–215. https://doi.org/10.1007/s10530-023-03169-2

Elliott, S. H., Tullos, D. D., & Walter, C. (2019). Physical modeling of the feedbacks between a patch of flexible Reed Canarygrass (Phalaris arundinacea), wake hydraulics, and downstream deposition. *Environmental Fluid Mechanics*, *19*(1), 255–277. https://doi.org/10.1007/s10652-018-9622-8

González, E., Sher, A. A., Anderson, R. M., Bay, R. F., Bean, D. W., Bissonnete, G. J., et al. (2017). Vegetation response to invasive *Tamarix* control in southwestern U.S. rivers: A collaborative study including 416 sites. *Ecological Applications*, *27*(6), 1789–1804. https://doi.org/10.1002/eap.1566

Gurnell, A. M., Bertoldi, W., Francis, R. A., Gurnell, J., & Mardhiah, U. (2019). Understanding processes of island development on an island braided river over timescales from days to decades. *Earth Surface Processes and Landforms*, *44*(2), 624–640. https://doi.org/10.1002/esp.4494

Johnson, W. C. (1997). Equilibrium response of riparian vegetation to flow regulation in the Platte river, Nebraska. *Regulated Rivers: Research & Management*, *13*(5), 403–415. https://doi.org/10.1002/(sici)1099-1646(199709/10)13:5<403::aid-rrr465>3.0.co;2-u

Kolb, E., Legué, V., & Bogeat-Triboulot, M.-B. (2017). Physical root–soil interactions. *Physical Biology*, *14*(6), 065004. https://doi.org/10.1088/1478-3975/aa90dd

Kui, L., Stella, J. C., Diehl, R. M., Wilcox, A. C., Lightbody, A., & Sklar, L. S. (2019). Can environmental flows moderate riparian invasions? The influence of seedling morphology and density on scour losses in experimental floods. *Freshwater Biology*, *64*(3), 474–484. https://doi.org/10.1111/fwb.13235

Li, J., Claude, N., Tassi, P., Cordier, F., Vargas-Luna, A., Crosato, A., & Rodrigues, S. (2022). Effects of vegetation patch patterns on channel morphology: A numerical Study. *Journal of Geophysical Research: Earth Surface*, *127*(5), e2021JF006529. https://doi.org/10.1029/2021JF006529

Liffen, T., Gurnell, A. M., O'Hare, M. T., Pollen-Bankhead, N., & Simon, A. (2013). Associations between the morphology and biomechanical properties of Sparganium erectum: Implications for survival and ecosystem engineering. *Aquatic Botany*, *105*, 18–24. https://doi.org/10.1016/j.aquabot.2012.11.001

Mahoney, J. M., & Rood, S. B. (1992). Response of a hybrid poplar to water table decline in different substrates. *Forest Ecology and Management*, *54*(1–4), 141–156. https://doi.org/10.1016/0378-1127(92)90009-X

Martins, A. D., O'Callaghan, F., Bengough, A. G., Loades, K. W., Pasqual, M., Kolb, E., & Dupuy, L. X. (2020). The helical motions of roots are linked to avoidance of particle forces in soil. *New Phytologist*, *225*(6), 2356–2367. https://doi.org/10.1111/nph.16312

Mickovski, S. B., Bengough, A. G., Bransby, M. F., Davies, M. C. R., Hallett, P. D., & Sonnenberg, R. (2007). Material stiffness, branching pattern and soil matric potential affect the pullout resistance of model root systems. *European Journal of Soil Science*, *58*(6), 1471–1481. https://doi.org/10.1111/j.1365-2389.2007.00953.x

Naumburg, E., Mata-gonzalez, R., Hunter, R. G., Mclendon, T., & Martin, D. W. (2005). Phreatophytic vegetation and groundwater fluctuations: A review of Current research and application of ecosystem response modeling with an emphasis on great Basin vegetation. *Environmental Management*, *35*(6), 726–740. https://doi.org/10.1007/s00267-004-0194-7

Nepf, H. M. (1999). Drag, turbulence, and diffusion in flow through emergent vegetation. *Water Resources Research*, *35*(2), 479–489. https://doi.org/10.1029/1998WR900069

Nikora, N., Nikora, V., & O'Donoghue, T. (2013). Velocity profiles in vegetated open-channel flows: Combined effects of multiple mechanisms. *Journal of Hydraulic Engineering*, *139*(10), 1021–1032. https://doi.org/10.1061/(ASCE)HY.1943-7900.0000779

Pollen, N., & Simon, A. (2005). Estimating the mechanical effects of riparian vegetation on stream bank stability using a fiber bundle model. *Water Resources Research*, *41*(7). https://doi.org/10.1029/2004WR003801

Pollen-Bankhead, N., & Simon, A. (2009). Enhanced application of root-reinforcement algorithms for bank-stability modeling. *Earth Surface Processes and Landforms*, *34*(4), 471–480. https://doi.org/10.1002/esp.1690

Potyondy, J. G. (1961). Skin friction between various soils and construction materials. *Géotechnique*, *11*(4), 339–353. https://doi.org/10.1680/geot.1961.11.4.339

Rominger, J. T., Lightbody, A. F., & Nepf, H. M. (2010). Effects of added vegetation on sand bar stability and stream hydrodynamics. *Journal of Hydraulic Engineering*, *136*(12), 994–1002. https://doi.org/10.1061/(ASCE)HY.1943-7900.0000215

Schwarz, M., Cohen, D., & Or, D. (2010). Root-soil mechanical interactions during pullout and failure of root bundles. *Journal of Geophysical Research*, *115*(F4), F04035. https://doi.org/10.1029/2009JF001603

Schwarz, M., Cohen, D., & Or, D. (2011). Pullout tests of root analogs and natural root bundles in soil: Experiments and modeling. *Journal of Geophysical Research*, *116*(F2), 2010JF001753. https://doi.org/10.1029/2010JF001753

Scott, M. L., Friedman, J. M., & Auble, G. T. (1996). Fluvial process and the establishment of bottomland trees. *Geomorphology*, *14*(4), 327–339. https://doi.org/10.1016/0169-555X(95)00046-8

Shafroth, P. B., Auble, G. T., & Scott, M. L. (1995). Germination and Establishment of the Native Plains Cottonwood (*Populus deltoides* Marshall subsp. *monilifera*) and the exotic russian-olive (*Elaeagnus angustifolia* L.). *Conservation Biology*, *9*(5), 1169–1175. https://doi.org/10.1046/j.1523-1739.1995.9051159.x-i1

Shafroth, P. B., Wilcox, A. C., Lytle, D. A., Hickey, J. T., Andersen, D. C., Beauchamp, V. B., et al. (2010). Ecosystem effects of environmental flows: Modelling and experimental floods in a dryland river. *Freshwater Biology*, *55*(1), 68–85. https://doi.org/10.1111/j.1365-2427.2009.02271.x

Silverberg, J. L., Noar, R. D., Packer, M. S., Harrison, M. J., Henley, C. L., Cohen, I., & Gerbode, S. J. (2012). 3D imaging and mechanical modeling of helical buckling in *Medicago truncatula* plant roots. *Proceedings of the National Academy of Sciences*, *109*(42), 16794–16799. https://doi.org/10.1073/pnas.1209287109

Solari, L., Van Oorschot, M., Belletti, B., Hendriks, D., Rinaldi, M., & Vargas-Luna, A. (2016). Advances on modelling riparian Vegetation—Hydromorphology interactions. *River Research and Applications*, *32*(2), 164–178. https://doi.org/10.1002/rra.2910

Stromberg, J. C., Beauchamp, V. B., Dixon, M. D., Lite, S. J., & Paradzick, C. (2007). Importance of low-flow and high-flow characteristics to restoration of riparian vegetation along rivers in arid south-western United States. *Freshwater Biology*, *52*(4), 651–679. https://doi.org/10.1111/j.1365-2427.2006.01713.x

Taye, J., Kibler, K. M., Thenuwara, M., & Barrera, C. K. R. (2026). Anchoring and root Architecture influence hydro-morphodynamic mechanisms of dislodgement in mangrove (*Rhizophora mangle*) seedlings. *Journal of Geophysical Research: Earth Surface*, *131*(2), e2025JF008419. https://doi.org/10.1029/2025JF008419

Tozzi, E. S., Easlon, H. M., & Richards, J. H. (2013). Interactive effects of water, light and heat stress on photosynthesis in Fremont cottonwood. *Plant, Cell and Environment*, *36*(8), 1423–1434. https://doi.org/10.1111/pce.12070

Tranmer, A. W., Benjankar, R., & Tonina, D. (2020). Post-wildfire riparian forest recovery processes along a regulated river corridor. *Forest Ecology and Management*, *478*, 118513. https://doi.org/10.1016/j.foreco.2020.118513

Tranmer, A. W., Benjankar, R., Vidergar, D., & Tonina, D. (2023). Identifying failure mechanisms of native riparian forest regeneration in a variable-width floodplain using a spatially-distributed riparian forest recruitment model. *Ecological Engineering*, *187*, 106865. https://doi.org/10.1016/j.ecoleng.2022.106865

Tranmer, A. W., Ji, U., Ahn, M., Jung, S. H., & Yager, E. M. (2024). Characterizing erosion and deposition in and around riparian vegetation patches: Complex flow hydraulics, sediment supply, and morphodynamic feedbacks. *Water Resources Research*, *60*(2), e2023WR034859. https://doi.org/10.1029/2023WR034859

Tron, S., Laio, F., & Ridolfi, L. (2014). Effect of water table fluctuations on phreatophytic root distribution. *Journal of Theoretical Biology*, *360*, 102–108. https://doi.org/10.1016/j.jtbi.2014.06.035

Vargas-Luna, A., Duró, G., Crosato, A., & Uijttewaal, W. (2019). Morphological adaptation of River channels to vegetation establishment: A laboratory Study. *Journal of Geophysical Research: Earth Surface*, *124*(7), 1981–1995. https://doi.org/10.1029/2018JF004878

Wu, H., Cheng, N., & Chiew, Y. (2021). Bed-Load transport in vegetated flows: Phenomena, parametrization, and prediction. *Water Resources Research*, *57*(4), e2020WR028143. https://doi.org/10.1029/2020WR028143

Yager, E. M. (2026). Seedling pullout data [Dataset]. *Mendeley Data, V1*. https://doi.org/10.17632/nv8d639cv9.1

Yager, E. M., & Schmeeckle, M. W. (2013). The influence of vegetation on turbulence and bed load transport. *Journal of Geophysical Research: Earth Surface*, *118*(3), 1585–1601. https://doi.org/10.1002/jgrf.20085

Yager, E. M., Schmeeckle, M. W., & Badoux, A. (2018). Resistance is not futile: Grain resistance controls on observed critical shields stress variations. *Journal of Geophysical Research: Earth Surface*, *123*(12), 3308–3322. https://doi.org/10.1029/2018JF004817

Yager, E. M., Turowski, J. M., Rickenmann, D., & McArdell, B. W. (2012). Sediment supply, grain protrusion, and bedload transport in mountain streams. *Geophysical Research Letters*, *39*(10), L10402. https://doi.org/10.1029/2012GL051654

Yamasaki, T. N., De Lima, P. H. S., Silva, D. F., Preza, C. G., Janzen, J. G., & Nepf, H. M. (2019). From patch to channel scale: The evolution of emergent vegetation in a channel. *Advances in Water Resources*, *129*, 131–145. https://doi.org/10.1016/j.advwatres.2019.05.009

Yang, J. Q., Chung, H., & Nepf, H. M. (2016). The onset of sediment transport in vegetated channels predicted by turbulent kinetic energy. *Geophysical Research Letters*, *43*(21), 11261–11268. https://doi.org/10.1002/2016GL071092

Yang, J. Q., Kerger, F., & Nepf, H. M. (2015). Estimation of the bed shear stress in vegetated and bare channels with smooth beds. *Water Resources Research*, *51*(5), 3647–3663. https://doi.org/10.1002/2014WR016042

Zhu, J., Leung, A. K., & Wang, Y. (2022). Modelling root–soil mechanical interaction considering root pull-out and breakage failure modes. *Plant and Soil*, *480*(1–2), 675–701. https://doi.org/10.1007/s11104-022-05613-z

Zong, L., & Nepf, H. (2011). Spatial distribution of deposition within a patch of vegetation. *Water Resources Research*, *47*(3). https://doi.org/10.1029/2010WR009516

References From the Supporting Information

Aberle, J., & Järvelä, J. (2013). Flow resistance of emergent rigid and flexible floodplain vegetation. *Journal of Hydraulic Research*, *51*(1), 33–45. https://doi.org/10.1080/00221686.2012.754795

Beard, D. C., & Weyl, P. K. (1973). Influence of texture on porosity and permeability of unconsolidated sand. *AAPG Bulletin*, *57*(2), 349–369. https://doi.org/10.1306/819A4272-16C5-11D7-8645000102C1865D

Fall, A., Weber, B., Pakpour, M., Lenoir, N., Shahidzadeh, N., Fiscina, J., et al. (2014). Sliding friction on wet and dry sand. *Physical Review Letters*, *112*(17), 175502. https://doi.org/10.1103/PhysRevLett.112.175502

Järvelä, J. (2004). Determination of flow resistance caused by non-submerged woody vegetation. *International Journal of River Basin Management*, *2*(1), 61–70. https://doi.org/10.1080/15715124.2004.9635222

Liefferink, R. W., Weber, B., & Bonn, D. (2018). Ploughing friction on wet and dry sand. *Physical Review E*, *98*(5), 052903. https://doi.org/10.1103/PhysRevE.98.052903

Pollen, N. (2007). Temporal and spatial variability in root reinforcement of streambanks: Accounting for soil shear strength and moisture. *Catena*, *69*(3), 197–205. https://doi.org/10.1016/j.catena.2006.05.004

Shafroth, P. B., Stromberg, J. C., & Patten, D. T. (2002). Riparian vegetation response to altered disturbance and stress regimes. *Ecological Applications*, *12*(1), 107–123. https://doi.org/10.1890/1051-0761(2002)012%255B0107:RVRTAD%255D2.0.CO;2

Sher, A. A., Marshall, D. L., & Taylor, J. P. (2002). Establishment patterns of native Populus and Salix in the presence of invasive nonnative Tamarix. *Ecological Applications*, *12*(3), 760–772. https://doi.org/10.1890/1051-0761(2002)012%255B0760:EPONPA%255D2.0.CO;2

Song, Y.-S., Hwang, W.-K., Jung, S.-J., & Kim, T.-H. (2012). A comparative study of suction stress between sand and silt under unsaturated conditions. *Engineering Geology*, *124*, 90–97. https://doi.org/10.1016/j.enggeo.2011.10.006

Whittaker, P., Wilson, C. A. M. E., & Aberle, J. (2015). An improved Cauchy number approach for predicting the drag and reconfiguration of flexible vegetation. *Advances in Water Resources*, *83*, 28–35. https://doi.org/10.1016/j.advwatres.2015.05.005

Wilcock, P. R., & Kenworthy, S. T. (2002). A two-fraction model for the transport of sand/gravel mixtures. *Water Resources Research*, *38*(10). https://doi.org/10.1029/2001WR000684